Grain boundary diffusion of ferropericlase: Implications for the core-mantle interaction

Yihang Peng[1], Pierre Hirel[2], Philippe Carrez[2], Jie Deng[1]

[1]Department of Geosciences, Princeton University, Princeton, NJ 08544, USA.
[2]Univ. Lille, F-59000 Lille, France.

Key Points:

- The grain boundary diffusivities of Mg, Fe, and O in ferropericlase are calculated from molecular dynamics simulations
- The grain boundary diffusivity first increases and then converges to a constant with increasing vacancy concentration
- Grain boundary diffusion is unlikely to be efficient enough for iron transport across the core-mantle boundary

Corresponding author: Yihang Peng, yhpeng@princeton.edu

Corresponding author: Jie Deng, jie.deng@princeton.edu

Abstract

Geophysical observations indicate that iron enrichment of various spatial scales may be present in the lowermost mantle. Various mechanisms have been proposed to explain the process of iron infiltration from the core to the mantle, though each with its own inherent limitations. Grain boundary (GB) diffusion significantly outpaces bulk diffusion within crystal interiors, and may facilitate iron transport across the core-mantle boundary (CMB). In this study, we investigate diffusion in two symmetric tilt GBs in ferropericlase using large-scale molecular dynamics simulations. The GB diffusivities of Mg and O of periclase as well as their temperature dependence agree well with previous studies. In addition, we study the GB diffusion of Fe in (Mg,Fe)O GBs for the first time. The results suggest that GB diffusion of Fe is likely to be sluggish near the CMB, and thus may not be an effective mechanism to transport iron from the core to the mantle.

Plain Language Summary

Seismic observations suggest the existence of regions rich in iron of scales from a few hundred meters to thousands of kilometers above the Earth's core-mantle boundary. The Earth's core, composed primarily of liquid iron, may interact with the mantle rocks and transport iron into the mantle. The diffusion of atoms along the boundaries of different grains of mantle rocks has been proposed as a possible mechanism for the core-mantle interaction. We performed atomistic simulations of one of the dominant mineral phases at the core-mantle boundary, (Mg,Fe)O ferropericlase to calculate the diffusion rates of magnesium, iron, and oxygen within grain boundary regions. The results suggest that, on the time scale of the Earth's history, the distance of the grain boundary diffusion of iron is likely to be very limited and insufficient to explain any iron enrichment phenomena at the bottom of the lower mantle.

1 Introduction

As the sharpest compositional discontinuity in the Earth's interior, the core-mantle boundary (CMB) at the depth of 2889 km exhibits strong complexity and has a significant impact on the chemical evolution of the Earth (Young & Lay, 1987). The interaction between the solid silicate mantle and the liquid iron core may cause extensive enrichment of iron at the lowermost mantle, which is supported by multiple geophysical observations. First, two continent-sized large low shear velocity provinces (LLSVPs) extend up to 1200 km above the CMB (Garnero et al., 2016) and can be explained by iron-enriched materials (Vilella et al., 2021; Yuan et al., 2023). They exhibit electrical conductivity anomalies (Nagao et al., 2003; Ohta et al., 2010) which may also be associated with iron. Second, the 5–40 km thick patches right above the core with unusually low seismic velocities, known as ultralow-velocity zones (ULVZs) (Williams & Garnero, 1996), may be attributed to local iron enrichment (Wicks et al., 2010). Third, a ~200-m-thick high conductance layer above the core has been inferred from Earth's nutations (Buffett, 1992; Buffett et al., 2002) and may comprise metallic FeO (Knittle & Jeanloz, 1986; Sherman, 1989).

Various hypotheses have been proposed to explain this putative iron enrichment above the CMB. The thickness of the iron-enriched layer caused by capillary rise is only < 20 m (Poirier et al., 1998). Alternative hypotheses suggest that pressure gradients caused by the dynamic topography at the CMB may drive iron upwards into the lower mantle (Kanda & Stevenson, 2006). Additionally, iron infiltration can be caused by the sedimentation of the liquid outer core (Buffett et al., 2000). However, both of them are sensitive to the viscosity of the lowermost mantle, which is subject to considerable uncertainty (Rudolph et al., 2015). Otsuka and Karato (2012) proposed that the penetration of iron into the mantle can be caused by a morphological instability, which is a mechanism independent of viscosity, but the effective diffusivity used to calculate iron infiltration thickness is extrapolated from low-pressure experimental data and remains controversial (J. Deng et al., 2019; Yoshino, 2019).

Grain boundaries (GBs) are regions that separate different grains in a polycrystalline material. Due to the more disordered atomistic structure at the interface compared to the crystalline lattice,

atomic diffusion along GBs is typically orders of magnitude faster than its lattice counterpart (Joesten, 1991; Dohmen & Milke, 2010). Therefore, GB diffusion strongly affects physical properties in the Earth's materials, including the viscosity (Mantisi et al., 2017), electrical conductivity (ten Grotenhuis et al., 2004), and seismic attenuation (Jackson et al., 2002). It is suggested that GB diffusion provides an efficient mechanism to exchange carbon and siderophile elements between the mantle and the core (Hayden & Watson, 2007, 2008), and may effectively modify the tungsten and helium isotopic compositions of the plume-source mantle (Yoshino et al., 2020; Ferrick & Korenaga, 2023). The diffusion of iron along GBs may be another potential mechanism for iron infiltration from the outer core to the lower mantle.

Previous experimental and theoretical studies have explored the GB diffusion in MgO periclase (McKenzie et al., 1971; Van Orman et al., 2003; Karki et al., 2015; Landuzzi et al., 2015; Riet et al., 2021). However, most of these results do not account explicitly for pressure and temperature conditions near the CMB, and the GB diffusion in (Mg,Fe)O, one of the most abundant phases at the CMB (X. Deng et al., 2023), remains poorly understood. In addition, recent results have shown that the structure of a GB is far from unique, and is not simply determined by the misorientation between the grains. In particular, GB structures evolve when interacting with vacancy complexes, resulting in significant changes in GB properties Hirel et al. (2022). In this study, we investigate the GB diffusion of Mg, Fe, and O along GB in (Mg,Fe)O bicrystals under the CMB conditions using large-scale molecular dynamics (MD) simulations. Bicrystals of high compaction, expected to be most favourable in high-pressure conditions of the CMB, are constructed (Hirel et al., 2019). We explore the dependence of the GB diffusion coefficient on defect concentration and temperature. The results are used to examine the efficiency of transporting iron from the core to the mantle through GB diffusion of (Mg,Fe)O ferropericlase.

2 Methods

2.1 Interatomic potential

There are two main methods to describe the interaction of atoms in MD simulations: *ab initio* method based on density functional theory and the force field approach. The *ab initio* method is considered more accurate because it calculates the electronic structure of material quantum mechanically, in principle, without relying on empirical parameters. However, this method is computationally demanding, limiting simulations to smaller systems and shorter times. On the other hand, the force field approach uses simplified force parameters, allowing for less intensive computations and enabling longer simulations of larger systems, which is crucial for simulating polycrystalline systems and reducing statistical error. Therefore, in this study, we choose the force field approach and use a new rigid-ion potential developed by Pedone et al. (2006). This approach incorporates long-range Coulomb interactions, a Morse function for short-range interactions, and a repulsive term similar to the Lennard-Jones function. The parameters were calibrated using experimental measurements, including lattice dimensions, elasticity values, both high-frequency and static dielectric constants, lattice energies, piezoelectric constants, and phonon frequencies observed in binary oxides. This potential demonstrates high reliability and applicability in modeling lattice defects, diffusion, and GBs in forsterite (Hirel et al., 2021; Furstoss et al., 2022). Hirel et al. (2021) highlight its ability to accurately reproduce various properties across a pressure range of 0 to 12 GPa, while Furstoss et al. (2022) further confirm its effectiveness through its good agreement with *ab initio* calculations in terms of GB atomistic structures, energies, and excess volumes in forsterite. To further verify the reliability of this potential for simulating (Mg,Fe)O GBs, we calculated the formation enthalpy of MgO GBs across pressure conditions of nearly the entire mantle (Figure S1). The results are in good agreement with Hirel et al. (2019), supporting the applicability of this potential to the periclase system at elevated pressures.

2.2 Molecular Dynamics Simulations

The GBs used in this study are symmetric tilt GBs where grains are rotated by opposite angles around the same [001] axis. Our focus is on structures with high-angle GBs as they are

more common in polycrystalline MgO (Saylor et al., 2003), likely more pertinent to understanding GB diffusion within the Earth's interior, and also more convenient to study (Riet et al., 2021). Bicrystals are constructed with Atomsk (Hirel, 2015). Two crystals of MgO are rotated by opposite angles ($\pm\alpha/2$), cut and then stacked together. We apply translation to one of the two symmetrical single crystals along the GB, and compute relative energies of different configurations, which yields several energy minima. Configurations corresponding to these minima can be called "complexions". As demonstrated earlier, at the high pressures reigning in the Earth's mantle, the most compact complexions are energetically most favourable (Hirel et al., 2019), and is used as a starting point. Such a compact complexion can interact with vacancy complexes, thus transforming its atomic configuration further (Hirel et al., 2022). In the following two symmetric tilt GB are modelled, corresponding to two different misorientation angles: $\alpha = 36.8°$ where the two crystals meet with {310} planes, and $\alpha = 29.5°$ where the GB plane does not correspond to any high-symmetry crystal plane. Mg-O vacancy pairs are randomly introduced within a region approximately 1 nm wide adjacent to the GB of the complexion to obtain the initial configuration of MgO bicrystals for the following MD simulations. The vacancy concentration C_{vac} is defined as the ratio between the number of MgO units removed and the number of MgO units in the 1-nm GB region. Following Ammann et al. (2010), the vacancy concentrations considered in this study range from 0.4 at% to 8.0 at%, which are estimated from experimental results (Holzapfel et al., 2003; Yamazaki & Irifune, 2003). The structure of (Mg,Fe)O is generated by the random substitution of Mg with different contents of Fe in the aforementioned MgO structure.

To ensure a genuine depiction of real material, (Mg,Fe)O single crystal must be of adequate size so that its inner structure mimics that of large grains (Glišović et al., 2015) in the lower mantle. We construct bicrystal systems containing over 50,000 atoms, resulting in an average distance of over 20 nm between the centers of adjacent grains. Each GB operates independently from others, ensuring that atoms involved in one boundary do not interact with any other boundaries throughout the simulation. A supercell with larger GB area has also been simulated and yields similar GB diffusion coefficients, confirming the size convergence of our systems (Figure S3).

All MD simulations are conducted using LAMMPS (Plimpton, 1995) under periodic boundary conditions. The systems are first equilibrated in isothermal-isobaric conditions (*NPT*) for 100 ps at a series of temperatures, under two pressures of 0 GPa and 140 GPa for MgO and (Mg,Fe)O, respectively. The resulting structures are then used as the initial configurations to set up the MD simulations for 5 ns under an canonical ensemble (*NVT*) with the Nosé-Hoover thermostat (Hoover, 1985), in order to evolve the GB structure to reach a steady state. Subsequently, we perform long *NVT* simulations for 5 to 10 ns, from which the GB diffusion is investigated. The timestep of all simulations is 1 fs.

2.3 Trajectory analysis

Due to the spatially heterogeneous diffusion in polycrystalline systems, a direct analysis of the MD trajectory of the entire system would mask the distinct characteristics of the crystal interiors and GBs. Following Riet et al. (2021), we employed an advanced local ionic environment analysis to extract the atomic properties within the GB regions from the bulk system. The first post-processing step is an energy minimization to map instantaneous MD configurations (sampling at 1-ns intervals) to their nearest local energy minima. Through this, we remove the thermal vibrational displacement of atoms and thereby obtain a more distinct representation of the GBs. Subsequently, we examine the distribution of nearest neighbors of all atoms at the energy minima to identify which atoms have complete coordination with the six nearest neighbors and which ones are undercoordinated. The undercoordinated atoms are associated with the GB regions (Riet et al., 2018). This analysis is realized through the nearest neighbor search using the MDAnalysis package (Michaud-Agrawal et al., 2011). Consistent with Riet et al. (2018) and Riet et al. (2021), the fraction of undercoordinated atoms at the GBs, denoted as g, remains relatively constant through a single MD trajectory. This insight allowed us to apply the modified Hart equation (Hart, 1957; Dohmen & Milke, 2010; Riet et al., 2021) to compute the GB diffusion coefficient:

$$D_{\text{total}} = gD_{\text{GB}} + (1 - g)D_{\text{vol}}, \tag{1}$$

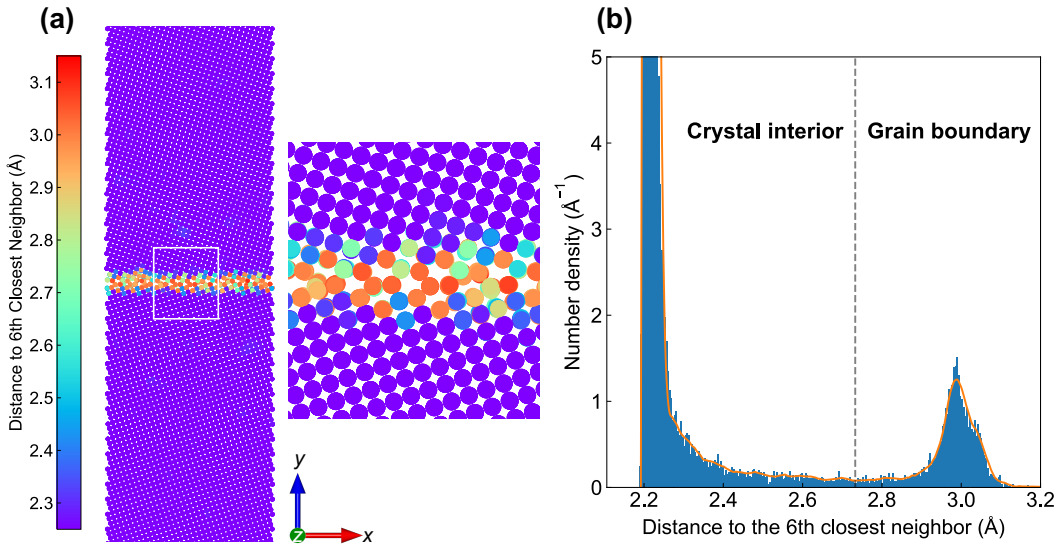

Figure 1. The local ionic environment analysis of MgO at 0 GPa and 2000 K. The results are derived from a snapshot of the MD simulation at 6 ns. The energy minimization is applied to remove the thermal vibration of atoms. (a) The color mapping of the distances from a central ion to its 6th closest neighbor. The view is perpendicular to the rotation angle of the grain boundaries. The atoms enclosed by the white frame are zoomed in to show details. (b) Distributions of distances from a central ion to its 6th closest neighbor. The orange curve is the smoothed histogram using the Savitzky-Golay filter (Savitzky & Golay, 1964), and its minimum value between the two peaks is used to determine the cutoff distance.

where D_{total}, D_{GB}, and D_{vol} are the overall diffusion coefficient, GB diffusion coefficient, and volume diffusion coefficient within the single crystal interiors, respectively. Since our analysis of atoms within crystal interiors showed negligible diffusion, we assume $D_{\text{vol}} \approx 0$. Thus, the GB diffusion coefficient is approximated by:

$$D_{\text{GB}} = \frac{D_{\text{total}}}{g} \tag{2}$$

D_{total} can be easily derived as the slope of mean square displacement (MSD) using the Einstein diffusion relation

$$D_{\text{total}} = \lim_{t\to\infty} \frac{\text{MSD}}{6t} = \lim_{t\to\infty} \frac{\left\langle [\vec{r}\,(t+t_0) - \vec{r}\,(t_0)]^2 \right\rangle_\alpha}{6t}, \tag{3}$$

where $\vec{r}(t)$ is the particle trajectories continuous in Cartesian space, and $\langle \cdots \rangle_\alpha$ represents an average over atoms of species α (Mg, Fe, O) and over time with different origins (Karki, 2015). Only when the MSD is a linear function of time do we intercept the segment of MSD and calculate the diffusion coefficient by linear fitting. The temperature-dependent diffusion coefficient can be fitted using the Arrhenius equation,

$$D = D_0 \mathrm{e}^{-\frac{\Delta H}{RT}}, \tag{4}$$

where D_0 is the pre-exponential factor, R is the ideal gas constant, and ΔH is the activation enthalpy.

3 Results and Discussion

3.1 Identification of grain boundary atoms

In this study, we analyze the structure of the GB and identify the GB atoms by examining the local ionic environments following Riet et al. (2021). In the ferropericlase or magnesiowüstite phase

of (Mg,Fe)O, ions within the grain typically have six equidistant nearest neighbors. In contrast, ions at the GB exhibit a non-crystalline local environment with varying distances to neighboring ions and often less than six nearest neighbors. Figure 1a shows the color mapping of the distances from a central ion to its sixth-closest neighbor in a snapshot of the MD trajectory of MgO at 0 GPa and 2000 K, in which the atoms associated with the GB region are clearly presented (i.e., atoms that are not colored purple). The distribution of distances from a central ion to its sixth-closest ion at energy minima structures is shown in Figure 1b, which exhibits a bimodal pattern. The first peak in this distribution indicates ions with six neighbors, characteristic of atoms within a single crystal, not in a GB. The adjacent shoulder on this peak represents atoms near the GB, where relaxation can lead to slightly longer bond distances compared to the crystal interior. The second peak signifies ions that are undercoordinated, typically having five or fewer neighbors, and are located in the GB region. We set the minimum point between the first and second peaks as the cutoff distance for each system to differentiate between internal and GB ions following Riet et al. (2021).

3.2 Grain boundary diffusivity

In this section, we discuss the GB diffusion coefficients in MgO at ambient pressure, and in (Mg,Fe)O at 140 GPa, calculated using Equation 2 and Equation 3. The MSD data from all the simulations in this study can be found in Figure S4 in Supporting Information. Taking pure MgO as an example, we explore how the GB diffusion coefficients of Mg and O vary with C_{vac}, system size, and the misorientation angle of the GB (see Text S1 in Supporting Information). This preliminary study allowed us to determine that fully converged results are obtained when C_{vac} reaches 3.2 at% or above, hence, only the diffusivity data at this concentration are presented in the following.

3.2.1 MgO at 0 GPa

Figure 2 summarizes the GB diffusion coefficients of MgO as a function of temperature at ambient pressure. To ensure convergence, we adopt a defect concentration of 3.2 at% to constrain the upper bound of the diffusivity (see Text S1 in Supporting Information). Our results generally agree well with previous theoretical studies using molecular dynamics simulations, and fall between the results of Riet et al. (2021) and Landuzzi et al. (2015) for both Mg and O. McKenzie et al. (1971) experimentally obtained $\frac{\delta D_{\mathrm{GB}}}{\sqrt{D_{\mathrm{vol}}}}$ for oxygen diffusion in periclase at around 2000 K, where δ is the GB width. However, since the value of D_{vol} in MgO remains poorly constrained, it is difficult to directly compare experimentally inferred GB diffusivity with our simulation outcomes. Riet et al. (2021) estimated that δD_{GB} of oxygen lies between 4×10^{-23} m^3 s^{-1} and 2×10^{-21} m^3 s^{-1}, based on the highest and lowest D_{vol} values reported in the literature (Oishi & Kingery, 1960; Yang & Flynn, 1994) and experimental measurements (McKenzie et al., 1971). Our result for $C_{\mathrm{vac}} = 3.2$ at% is $\sim 4 \times 10^{-21}$ m^3 s^{-1}, slightly higher than this range. However, the C_{vac} in pure MgO is significantly lower compared to (Mg,Fe)O due to the absence of multivalent ions (Van Orman et al., 2003; Ammann et al., 2010). Considering lower vacancy concentrations of $C_{\mathrm{vac}} < 0.8$ at%, our simulation results fall within the range of experimental estimates.

The GB diffusion coefficients increase significantly with temperature, and can be well fitted by Equation 4 (dashed lines in Fig. 2). The activation enthalpies for Mg and O are 229($\pm$10) kJ mol^{-1} and 217($\pm$64) kJ mol^{-1}, respectively. The only experimental results of the activation enthalpy for GB diffusion of O is 230 kJ mol^{-1} (measured at 1380–1800 K, Passmore et al., 1966), which our simulations match closely. Karki et al. (2015) reported the activation enthalpies for Mg (221 kJ mol^{-1}) and O (212 kJ mol^{-1}) migration along the $\{410\}$ symmetric boundaries of MgO bicrystals at 0 GPa using *ab initio* calculations. Similar results were obtained by Harris et al. (1997) using MD simulations with empirical potentials. Our simulation results also align very well with these theoretical predictions that assumed *ad hoc* diffusion pathways. It is noteworthy that in the bulk crystal of periclase, the diffusion activation enthalpy of Mg is smaller than that of O (Ammann et al., 2010), while in the GB, they are quite similar and the activation enthalpy of O is slightly smaller. This may be related to the markedly different chemical environments at the GBs compared to the interior of the crystal. In summary, the GB diffusion properties of MgO at ambient pressure obtained from this study are consistent with previous theoretical and experimental data.

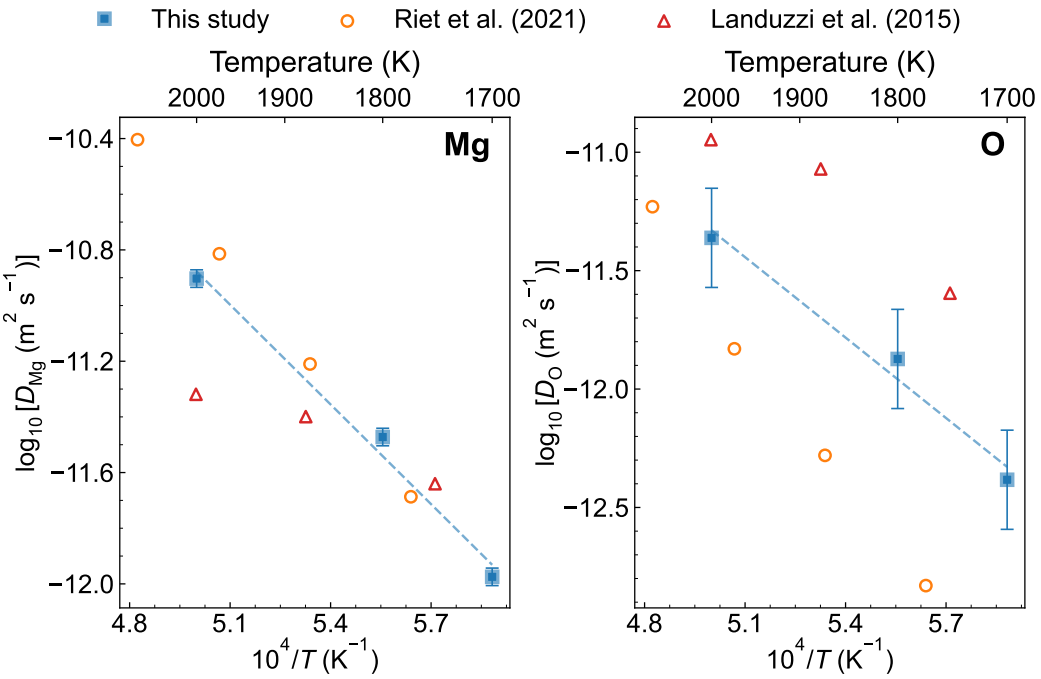

Figure 2. Grain boundary diffusion coefficients of Mg (left) and O (right) as a function of reciprocal temperature (1700 K, 1800 K, and 2000 K) in MgO with a C_{vac} of 3.2 at% at ambient pressure. The error bars are estimated from the error bars in Figure S2, assuming the same relative standard deviation for each element. Results from previous theoretical studies are plotted in open symbols for comparison (Riet et al., 2021; Landuzzi et al., 2015). Dashed lines are fitted Arrhenius functions (Equation 4).

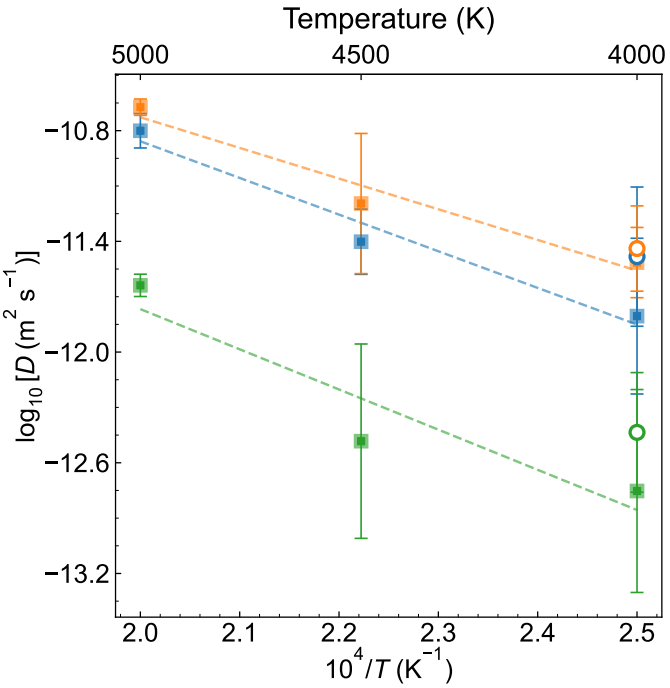

Figure 3. Grain boundary diffusion coefficients as a function of reciprocal temperature (4000 K, 4500 K, and 5000 K) in $(Mg_{0.9}Fe_{0.1})O$ (solid squares) and $(Mg_{0.16}Fe_{0.84})O$ (open circles) with a C_{vac} of 3.2 at% at 140 GPa. The diffusivity of Mg, Fe, and O are shown in blue, orange, and green, respectively. The error bars represent 2SD of the diffusion coefficients calculated from four 5-ns-long MD trajectories. Dashed lines are fitted Arrhenius functions (Equation 4).

3.2.2 (Mg,Fe)O at 140 GPa

The high-pressure diffusion coefficients of Mg, Fe, and O in (Mg,Fe)O with two different iron contents are shown in Figure 3. For $(Mg_{0.9}Fe_{0.1})O$ ferropericlase, the simulation temperatures are set between 4000 to 5000 K, corresponding to the upper bounds of the estimated CMB temperatures throughout the Earth's thermal evolution (Andrault et al., 2016). $(Mg_{0.16}Fe_{0.84})O$ magnesiowüstite is taken as a prototype Fe-rich material that has been suggested to be the main constituent of ULVZs (Wicks et al., 2010, 2017) and the high conductance layer (Buffett, 1992; Knittle & Jeanloz, 1986), and consequently it may serve as an important medium for the iron transport from the outer core to the lower mantle. Recent studies suggest that the melting point of FeO wüstite under CMB pressure conditions reaches up to 4140 K (Dobrosavljevic et al., 2023), indicating that our simulation temperature of 4000 K for $(Mg_{0.16}Fe_{0.84})O$ is below its solidus. Overall, the diffusion coefficients slightly increase with iron content, and the order of diffusion coefficients for the three elements follows $D_{GB}^{Fe} \approx> D_{GB}^{Mg} > D_{GB}^{O}$. We find that the diffusion coefficient of Mg is about an order of magnitude larger than that of O, closely aligning with the results of Riet et al. (2021). Furthermore, Fe and Mg have similar diffusion coefficients, both significantly larger than O, which is consistent with the MD data for GB diffusion in olivine (Mantisi et al., 2017). This suggests that the relative magnitudes of GB diffusion coefficients for different elements are, to a large extent, controlled by ionic radii, considering that the ionic radii of Fe^{2+}, Mg^{2+}, and O^{2-} are 75, 86, and 126 pm, respectively (Slater, 1964). Due to the steric effect (Nalwa, 2001), smaller ions are better suited to move through available space to facilitate diffusion. We find that the uncertainty of the diffusion coefficients at 5000 K is much smaller than at lower temperatures, which may be due to the more stable premelting state of the GBs at higher temperatures, reducing the variation in diffusivity. Regarding the temperature dependence, the diffusion activation enthalpies for Mg, Fe, and O are 448(±63) kJ mol^{-1}, 328(±37)

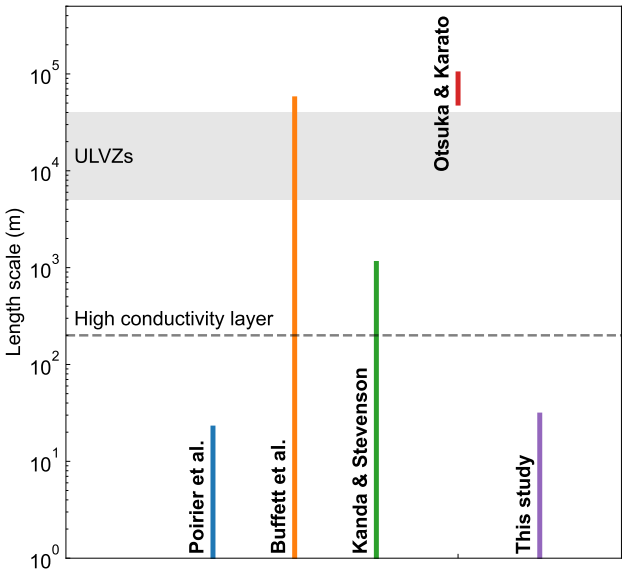

Figure 4. Length scale of iron transport from the core to the mantle compared to length scales of high conductance layer and ULVZs. Different iron infiltration mechanisms are shown for comparison (Poirier et al., 1998; Buffett et al., 2000; Kanda & Stevenson, 2006; Otsuka & Karato, 2012).

kJ mol^{-1}, and 479(±97) kJ mol^{-1}, respectively. Due to the pressure effect on diffusion, they are significantly higher than the activation enthalpies for MgO under ambient pressure.

4 Implications

To explore the upper limit of the efficiency of iron transport via the GB diffusion mechanism, we consider the maximum diffusivity of iron in Figure 3 (2.1×10^{-11} m^2 s^{-1}) for the subsequent calculations. The effective diffusion coefficient for a polycrystalline material can be estimated using this equation (Balluffi et al., 2005):

$$D_{\text{eff}}^{\text{Fe}} = D_{\text{vol}}^{\text{Fe}} + \frac{3\delta}{d} D_{\text{GB}}^{\text{Fe}}, \tag{5}$$

where δ is the GB width (~1 nm) and d is the grain size (0.01–10 mm, Glišović et al., 2015) in the lower mantle. For pure MgO periclase, the D_{vol} values of Mg and O under the CMB conditions are very small and can be negligible (less than 10^{-20} m^2 s^{-1}, Ita & Cohen, 1998), while in the presence of Fe, higher vacancy concentrations might lead to faster lattice diffusion of Mg, O, and Fe (Ammann et al., 2010). We extract the actual contribution of GB diffusion to the effective diffusion coefficient by setting $D_{\text{vol}}^{\text{Fe}} = 0$, and obtain the characteristic length scale of the iron transport through GB diffusion:

$$L_{\text{GB}}^{\text{eff}} = \sqrt{\frac{3\delta}{d} D_{\text{GB}}^{\text{Fe}} t}, \tag{6}$$

where the time scale t is set to the age of the Earth (4.54 Gyr, Dalrymple, 2001). The result of $L_{\text{GB}}^{\text{eff}}$ does not exceed 30 m, as shown in Figure 4. Other iron infiltration mechanisms proposed by previous studies, including capillary rise (Poirier et al., 1998), suction (Kanda & Stevenson, 2006), upward sedimentation of outer core alloys (Buffett et al., 2000), and morphological instability (Otsuka & Karato, 2012) are also plotted for comparison. The results indicate that the effective transport distance of Fe through GB diffusion in (Mg,Fe)O is likely to be quite small, considering the transport distances of other mechanisms and the spatial scales of ULVZs and the high conductance layer. To further validate this finding, we solve Fick's second law of diffusion to calculate the concentration

profile of iron in the mantle:

$$\frac{\partial C}{\partial t} = -\frac{3\delta}{d} D_{\mathrm{GB}}^{\mathrm{Fe}} \nabla^2 C \tag{7}$$

Assuming that the core always maintains a composition of pure iron, and considering an initial condition of zero Fe concentration in the mantle, we obtained the concentration distribution of iron in the mantle after the GB diffusion of 4.54 Gyr. The total mass of Fe that has been transported to the mantle is 5.1×10^{19} kg, which can only account for less than 20 wt% of the ~200-m-high conductance layer.

At the CMB, not only (Mg,Fe)O but also silicate minerals such as bridgmanite and post-perovskite are present. Given that lattice diffusion of elements in silicate perovskite is much slower than in ferropericlase (Ammann et al., 2010; Holzapfel et al., 2003, 2005), we argue that GB diffusion is unlikely to be an effective mechanism to transport Fe from the core to the lower mantle. Considering that some siderophile elements (e.g., W) have larger atomic radii and mass than Fe, we speculate that their GB diffusion coefficients in (Mg,Fe)O might be even smaller than that of Fe. So far the only data available for comparison are experimental results under relatively low pressures (Hayden & Watson, 2007; Yoshino et al., 2020). Therefore, more studies are needed to accurately quantify the efficiency of GB diffusion in exchanging siderophile elements across the CMB to elucidate the scale and extent of the core-mantle interaction.

5 Open Research

Data used in this study are available at Peng and Deng (2024). The software LAMMPS used in this study is developed openly at `https://github.com/lammps/lammps` and available at Plimpton et al. (2021).

Acknowledgments

This work was funded by the National Science Foundation under Grant EAR-2242946. The simulations presented in this article were performed on computational resources managed and supported by Princeton Research Computing, a consortium of groups including the Princeton Institute for Computational Science and Engineering (PICSciE) and the Office of Information Technology's High Performance Computing Center and Visualization Laboratory at Princeton University.

References

Ammann, M. W., Brodholt, J. P., Wookey, J., & Dobson, D. P. (2010). First-principles constraints on diffusion in lower-mantle minerals and a weak D″ layer. *Nature*, *465*(7297), 462–465. doi: 10.1038/nature09052

Andrault, D., Monteux, J., Le Bars, M., & Samuel, H. (2016, June). The deep Earth may not be cooling down. *Earth and Planetary Science Letters*, *443*, 195–203. Retrieved 2024-04-08, from `https://www.sciencedirect.com/science/article/pii/S0012821X16301078` doi: 10.1016/j.epsl.2016.03.020

Balluffi, R. W., Allen, S. M., Carter, W. C., & Kemper, R. A. (2005). *Kinetics of materials*. Hoboken, N.J: J. Wiley & Sons.

Buffett, B. A. (1992). Constraints on magnetic energy and mantle conductivity from the forced nutations of the Earth. *Journal of Geophysical Research: Solid Earth*, *97*(B13), 19581–19597. doi: 10.1029/92JB00977

Buffett, B. A., Garnero, E. J., & Jeanloz, R. (2000, November). Sediments at the Top of Earth's Core. *Science*, *290*(5495), 1338–1342. doi: 10.1126/science.290.5495.1338

Buffett, B. A., Mathews, P. M., & Herring, T. A. (2002). Modeling of nutation and precession: Effects of electromagnetic coupling. *Journal of Geophysical Research: Solid Earth*, *107*(B4), ETG 5–1–ETG 5–14. doi: 10.1029/2000JB000056

Dalrymple, G. B. (2001, January). The age of the Earth in the twentieth century: a problem (mostly) solved. *Geological Society, London, Special Publications*, *190*(1), 205–221. doi: 10.1144/GSL.SP.2001.190.01.14

Deng, J., Miyazaki, Y., & Lee, K. K. M. (2019). Implications for the Melting Phase Relations in the MgO-FeO System at Core-Mantle Boundary Conditions. *Journal of Geophysical Research: Solid Earth*, *124*(2), 1294–1304. doi: 10.1029/2018JB015499

Deng, X., Xu, Y., Hao, S., Ruan, Y., Zhao, Y., Wang, W., ... Wu, Z. (2023, June). Compositional and thermal state of the lower mantle from joint 3D inversion with seismic tomography and mineral elasticity. *Proceedings of the National Academy of Sciences*, *120*(26), e2220178120. doi: 10.1073/pnas.2220178120

Dobrosavljevic, V. V., Zhang, D., Sturhahn, W., Chariton, S., Prakapenka, V. B., Zhao, J., ... Jackson, J. M. (2023, November). Melting and defect transitions in FeO up to pressures of Earth's core-mantle boundary. *Nature Communications*, *14*(1), 7336. doi: 10.1038/s41467-023-43154-w

Dohmen, R., & Milke, R. (2010, January). Diffusion in Polycrystalline Materials: Grain Boundaries, Mathematical Models, and Experimental Data. *Reviews in Mineralogy and Geochemistry*, *72*(1), 921–970. doi: 10.2138/rmg.2010.72.21

Ferrick, A. L., & Korenaga, J. (2023, January). Long-term core–mantle interaction explains W-He isotope heterogeneities. *Proceedings of the National Academy of Sciences*, *120*(4), e2215903120. doi: 10.1073/pnas.2215903120

Furstoss, J., Hirel, P., Carrez, P., & Cordier, P. (2022, November). Complexions and stoichiometry of the 60.8°//[100](011) symmetrical tilt grain boundary in Mg2SiO4 forsterite: A combined empirical potential and first-principles study. *American Mineralogist*, *107*(11), 2034–2043. doi: 10.2138/am-2022-8420

Garnero, E. J., McNamara, A. K., & Shim, S.-H. (2016, July). Continent-sized anomalous zones with low seismic velocity at the base of Earth's mantle. *Nature Geoscience*, *9*(7), 481–489. doi: 10.1038/ngeo2733

Glišović, P., Forte, A. M., & Ammann, M. W. (2015). Variations in grain size and viscosity based on vacancy diffusion in minerals, seismic tomography, and geodynamically inferred mantle rheology. *Geophysical Research Letters*, *42*(15), 6278–6286. doi: 10.1002/2015GL065142

Harris, D. J., Watson, G. W., & Parker, S. C. (1997, November). Vacancy migration at the {410}/[001] symmetric tilt grain boundary of MgO: An atomistic simulation study. *Physical Review B*, *56*(18), 11477–11484. doi: 10.1103/PhysRevB.56.11477

Hart, E. W. (1957, October). On the role of dislocations in bulk diffusion. *Acta Metallurgica*, *5*(10), 597. doi: 10.1016/0001-6160(57)90127-X

Hayden, L. A., & Watson, E. B. (2007, November). A diffusion mechanism for core–mantle interaction. *Nature*, *450*(7170), 709–711. doi: 10.1038/nature06380

Hayden, L. A., & Watson, E. B. (2008, June). Grain boundary mobility of carbon in Earth's mantle: A possible carbon flux from the core. *Proceedings of the National Academy of Sciences*, *105*(25), 8537–8541. doi: 10.1073/pnas.0710806105

Hirel, P. (2015). Atomsk: A tool for manipulating and converting atomic data files. *Computer Physics Communications*, *197*, 212–219. doi: 10.1016/j.cpc.2015.07.012

Hirel, P., Carrez, P., & Cordier, P. (2022, November). Why do compact grain boundary complexions prevail in rock-salt materials? *Acta Materialia*, *240*, 118297. doi: 10.1016/j.actamat.2022.118297

Hirel, P., Furstoss, J., & Carrez, P. (2021, November). A critical assessment of interatomic potentials for modelling lattice defects in forsterite Mg$$_2$$SiO$$_4$$from 0 to 12 GPa. *Physics and Chemistry of Minerals*, *48*(12), 46. doi: 10.1007/s00269-021-01170-6

Hirel, P., Moladje, G. F. B., Carrez, P., & Cordier, P. (2019, January). Systematic theoretical study of [001] symmetric tilt grain boundaries in MgO from 0 to 120 GPa. *Physics and Chemistry of Minerals*, *46*(1), 37–49. doi: 10.1007/s00269-018-0985-7

Holzapfel, C., Rubie, D. C., Frost, D. J., & Langenhorst, F. (2005). Fe-Mg interdiffusion in (Mg,Fe)SiO_3 perovskite and lower mantle reequilibration. *Science (New York, N.Y.)*, *309*(5741), 1707–1710. doi: 10.1126/science.1111895

Holzapfel, C., Rubie, D. C., Mackwell, S., & Frost, D. J. (2003, September). Effect of pressure on Fe–Mg interdiffusion in (Fe_xMg_{1-x})O, ferropericlase. *Physics of the Earth and Planetary Interiors*, *139*(1), 21–34. doi: 10.1016/S0031-9201(03)00142-0

Hoover, W. G. (1985). Canonical dynamics - equilibrium phase-space distributions. *Physical Review*

A, *31*(3), 1695–1697. doi: 10.1103/PhysRevA.31.1695

Ita, J., & Cohen, R. E. (1998). Diffusion in MgO at high pressure: Implications for lower mantle rheology. *Geophysical Research Letters*, *25*(7), 1095–1098. doi: 10.1029/98GL50564

Jackson, I., Fitz Gerald, J. D., Faul, U. H., & Tan, B. H. (2002). Grain-size-sensitive seismic wave attenuation in polycrystalline olivine. *Journal of Geophysical Research: Solid Earth*, *107*(B12), ECV 5–1–ECV 5–16. doi: 10.1029/2001JB001225

Joesten, R. (1991). Grain-Boundary Diffusion Kinetics in Silicate and Oxide Minerals. In J. Ganguly (Ed.), *Diffusion, Atomic Ordering, and Mass Transport: Selected Topics in Geochemistry* (pp. 345–395). New York, NY: Springer US. doi: 10.1007/978-1-4613-9019-0_11

Kanda, R. V. S., & Stevenson, D. J. (2006). Suction mechanism for iron entrainment into the lower mantle. *Geophysical Research Letters*, *33*(2). doi: 10.1029/2005GL025009

Karki, B. B. (2015). First-principles computation of mantle materials in crystalline and amorphous phases. *Physics of the Earth and Planetary Interiors*, *240*, 43–69. doi: 10.1016/j.pepi.2014.11.004

Karki, B. B., Ghosh, D. B., & Verma, A. K. (2015, May). First-principles prediction of pressure-enhanced defect segregation and migration at MgO grain boundaries†. *American Mineralogist*, *100*(5-6), 1053–1058. doi: 10.2138/am-2015-5143

Knittle, E., & Jeanloz, R. (1986). High-pressure metallization of FeO and implications for the Earth's core. *Geophysical Research Letters*, *13*(13), 1541–1544. doi: 10.1029/GL013i013p01541

Landuzzi, F., Pasquini, L., Giusepponi, S., Celino, M., Montone, A., Palla, P. L., & Cleri, F. (2015, March). Molecular dynamics of ionic self-diffusion at an MgO grain boundary. *Journal of Materials Science*, *50*(6), 2502–2509. doi: 10.1007/s10853-014-8808-9

Mantisi, B., Sator, N., & Guillot, B. (2017, December). Structure and transport at grain boundaries in polycrystalline olivine: An atomic-scale perspective. *Geochimica et Cosmochimica Acta*, *219*, 160–176. doi: 10.1016/j.gca.2017.09.026

McKenzie, D. R., Searcy, A. W., Holt, J. B., & Condit, R. H. (1971). Oxygen Grain-Boundary Diffusion in MgO. *Journal of the American Ceramic Society*, *54*(4), 188–190. doi: 10.1111/j.1151-2916.1971.tb12261.x

Michaud-Agrawal, N., Denning, E. J., Woolf, T. B., & Beckstein, O. (2011). MDAnalysis: A toolkit for the analysis of molecular dynamics simulations. *Journal of Computational Chemistry*, *32*(10), 2319–2327. doi: 10.1002/jcc.21787

Nagao, H., Iyemori, T., Higuchi, T., & Araki, T. (2003). Lower mantle conductivity anomalies estimated from geomagnetic jerks. *Journal of Geophysical Research: Solid Earth*, *108*(B5). doi: 10.1029/2002JB001786

Nalwa, H. S. (Ed.). (2001). *Handbook of surfaces and interfaces of materials*. San Diego: Academic Press.

Ohta, K., Hirose, K., Ichiki, M., Shimizu, K., Sata, N., & Ohishi, Y. (2010, January). Electrical conductivities of pyrolitic mantle and MORB materials up to the lowermost mantle conditions. *Earth and Planetary Science Letters*, *289*(3), 497–502. doi: 10.1016/j.epsl.2009.11.042

Oishi, Y., & Kingery, W. D. (1960). Oxygen Diffusion in Periclase Crystals. *The Journal of Chemical Physics*, *33*(3), 905–906. doi: 10.1063/1.1731286

Otsuka, K., & Karato, S.-i. (2012, December). Deep penetration of molten iron into the mantle caused by a morphological instability. *Nature*, *492*(7428), 243–246. doi: 10.1038/nature11663

Passmore, E. M., Duff, R. H., & Vasilos, T. (1966). Creep of Dense, Polycrystalline Magnesium Oxide. *Journal of the American Ceramic Society*, *49*(11), 594–600. doi: 10.1111/j.1151-2916.1966.tb13175.x

Pedone, A., Malavasi, G., Menziani, M. C., Cormack, A. N., & Segre, U. (2006, June). A New Self-Consistent Empirical Interatomic Potential Model for Oxides, Silicates, and Silica-Based Glasses. *The Journal of Physical Chemistry B*, *110*(24), 11780–11795. doi: 10.1021/jp0611018

Peng, Y., & Deng, J. (2024, March). *Grain boundary diffusion of ferropericlase: Implications for the core-mantle interaction* [Dataset]. Retrieved from `https://osf.io/2djyh/` doi: 10.17605/OSF.IO/2DJYH

Plimpton, S. (1995). Fast parallel algorithms for short-range molecular-dynamics. *Journal of Computational Physics*, *117*(1), 1–19. doi: 10.1006/jcph.1995.1039

Plimpton, S., Kohlmeyer, A., Thompson, A., Moore, S., & Berger, R. (2021, September). *LAMMPS Stable release 29 September 2021.* Zenodo. doi: 10.5281/zenodo.6386596

Poirier, J. P., Malavergne, V., & Le Mouël, J. L. (1998). Is there a thin electrically conducting layer at the base of the mantle? In M. Gurnis, M. E. Wysession, E. Knittle, & B. A. Buffett (Eds.), *Geodynamics Series* (Vol. 28, pp. 131–137). Washington, D. C.: American Geophysical Union. doi: 10.1029/GD028p0131

Riet, A. A., Van Orman, J. A., & Lacks, D. J. (2018, November). The interplay of structure and dynamics at grain boundaries. *The Journal of Chemical Physics*, *149*(19), 194501. doi: 10.1063/1.5052188

Riet, A. A., Van Orman, J. A., & Lacks, D. J. (2021, January). A molecular dynamics study of grain boundary diffusion in MgO. *Geochimica et Cosmochimica Acta*, *292*, 203–216. doi: 10.1016/j.gca.2020.09.012

Rudolph, M. L., Lekić, V., & Lithgow-Bertelloni, C. (2015, December). Viscosity jump in Earth's mid-mantle. *Science*, *350*(6266), 1349–1352. doi: 10.1126/science.aad1929

Savitzky, A., & Golay, M. J. E. (1964, July). Smoothing and Differentiation of Data by Simplified Least Squares Procedures. *Analytical Chemistry*, *36*(8), 1627–1639. doi: 10.1021/ac60214a047

Saylor, D. M., Morawiec, A., & Rohrer, G. S. (2003, August). Distribution of grain boundaries in magnesia as a function of five macroscopic parameters. *Acta Materialia*, *51*(13), 3663–3674. doi: 10.1016/S1359-6454(03)00181-2

Sherman, D. M. (1989). The nature of the pressure-induced metallization of FeO and its implications to the core-mantle boundary. *Geophysical Research Letters*, *16*(6), 515–518. doi: 10.1029/GL016i006p00515

Slater, J. C. (1964). Atomic radii in crystals. *Journal of Chemical Physics*, *41*(10), 3199. doi: 10.1063/1.1725697

ten Grotenhuis, S. M., Drury, M. R., Peach, C. J., & Spiers, C. J. (2004). Electrical properties of fine-grained olivine: Evidence for grain boundary transport. *Journal of Geophysical Research: Solid Earth*, *109*(B6). doi: 10.1029/2003JB002799

Van Orman, J. A., Fei, Y., Hauri, E. H., & Wang, J. (2003). Diffusion in MgO at high pressures: Constraints on deformation mechanisms and chemical transport at the core-mantle boundary. *Geophysical Research Letters*, *30*(2). doi: 10.1029/2002GL016343

Vilella, K., Bodin, T., Boukaré, C.-E., Deschamps, F., Badro, J., Ballmer, M. D., & Li, Y. (2021, January). Constraints on the composition and temperature of LLSVPs from seismic properties of lower mantle minerals. *Earth and Planetary Science Letters*, *554*, 116685. doi: 10.1016/j.epsl.2020.116685

Wicks, J. K., Jackson, J. M., & Sturhahn, W. (2010). Very low sound velocities in iron-rich (Mg,Fe)O: Implications for the core-mantle boundary region. *Geophysical Research Letters*, *37*(15). doi: 10.1029/2010GL043689

Wicks, J. K., Jackson, J. M., Sturhahn, W., & Zhang, D. (2017). Sound velocity and density of magnesiowüstites: Implications for ultralow-velocity zone topography. *Geophysical Research Letters*, *44*(5), 2148–2158. doi: 10.1002/2016GL071225

Williams, Q., & Garnero, E. J. (1996, September). Seismic Evidence for Partial Melt at the Base of Earth's Mantle. *Science*, *273*(5281), 1528–1530. doi: 10.1126/science.273.5281.1528

Yamazaki, D., & Irifune, T. (2003, November). Fe–Mg interdiffusion in magnesiowüstite up to 35 GPa. *Earth and Planetary Science Letters*, *216*(3), 301–311. doi: 10.1016/S0012-821X(03)00534-X

Yang, M. H., & Flynn, C. P. (1994, September). Intrinsic Diffusion Properties of an Oxide: MgO. *Physical Review Letters*, *73*(13), 1809–1812. doi: 10.1103/PhysRevLett.73.1809

Yoshino, T. (2019, February). Penetration of molten iron alloy into the lower mantle phase. *Comptes Rendus Geoscience*, *351*(2), 171–181. doi: 10.1016/j.crte.2018.06.013

Yoshino, T., Makino, Y., Suzuki, T., & Hirata, T. (2020, January). Grain boundary diffusion of W in lower mantle phase with implications for isotopic heterogeneity in oceanic island basalts by core-mantle interactions. *Earth and Planetary Science Letters*, *530*, 115887. doi: 10.1016/j.epsl.2019.115887

Young, C. J., & Lay, T. (1987). The Core-Mantle Boundary. *Annual Review of Earth and Planetary Sciences*, *15*(1), 25–46. doi: 10.1146/annurev.ea.15.050187.000325

Yuan, Q., Li, M., Desch, S. J., Ko, B., Deng, H., Garnero, E. J., . . . Asimow, P. D. (2023, November). Moon-forming impactor as a source of Earth's basal mantle anomalies. *Nature*, *623*(7985), 95–99. doi: 10.1038/s41586-023-06589-1